Electronic Supplementary Material (ESI) for Journal of Materials Chemistry A.

Supplementary information

Unprecedented high efficiency for photocatalytic conversion of methane into methanol over Au-Pd/TiO_2 – what is the role of each component in the system?

Xiaojiao Cai,[a] Siyuan Fang,[b] Yun Hang Hu[ab]*

[a] School of Environmental Science and Engineering, Shanghai Jiao Tong University, Shanghai 200240, People's Republic of China

[b] Department of Materials Science and Engineering, Michigan Technological University, Houghton, Michigan 49931-1295, United States

*Corresponding author: yunhangh@mtu.edu

1. X-ray diffraction patterns

As shown in Fig. S1, all the samples had similar XRD patterns. Characteristic peaks at 25.4°, 37.9°, 48.1°, 54.1°, 55.2°, 62.9°, and 75.2° are corresponding to (101), (004), (200), (105), (211), (204), and (215) planes of anatase TiO_2 (JCPDS, no.21-1272) respectively, while no peak due to rutile TiO_2 was observed. Characteristic diffraction peaks of Au or Pd were not observed either, indicating the high dispersion and small size of metal NPs. Furthermore, the peak corresponding to anatase TiO_2 (101) shifted to a higher diffraction angle after depositing Au-Pd alloy, implying a stronger affinity between Au-Pd alloy and TiO_2 compared with single Au and Pd NPs.

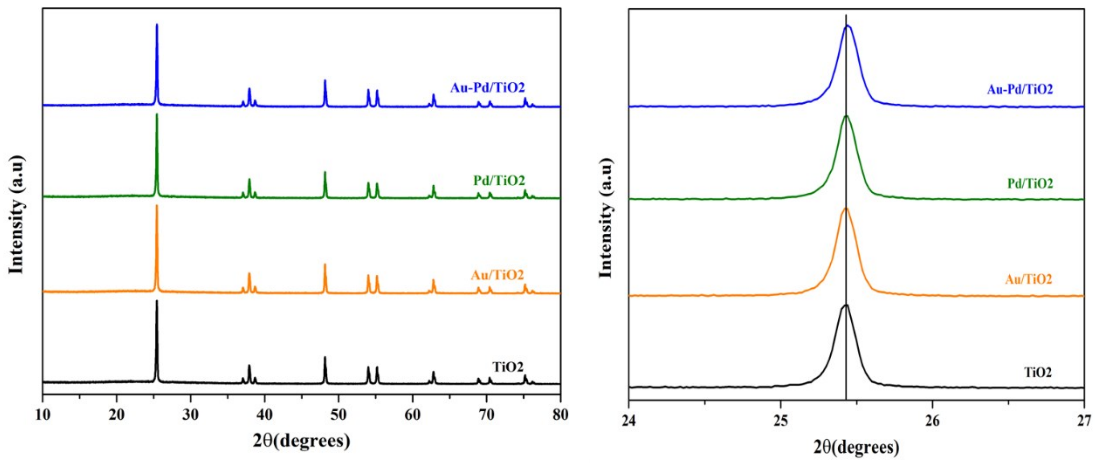

Fig. S1 XRD patterns of TiO_2, Au/TiO_2, Pd/TiO_2, and Au-Pd/TiO_2.

2. Photocatalytic methane oxidation over Au-Pd/TiO_2 with various Au-Pd loading amounts

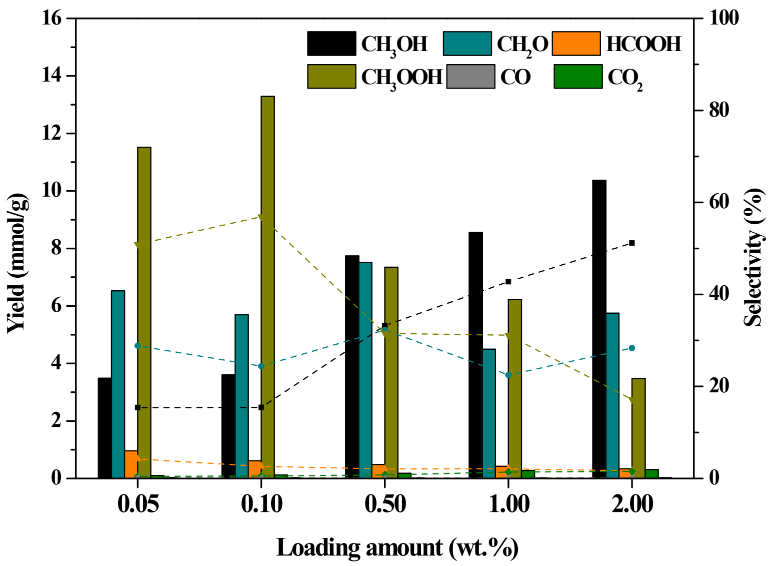

Fig. S2 Photocatalytic methane oxidation over Au-Pd/TiO_2 with various Au-Pd loading amounts under UV-visible light irradiation (5 mg catalyst, 30 mL water, 3.0 MPa CH_4, 1.0 MPa O_2, 1 h reaction).

3. TEM images of Au-Pd/TiO_2 with various Au-Pd loading amounts and their size distributions.

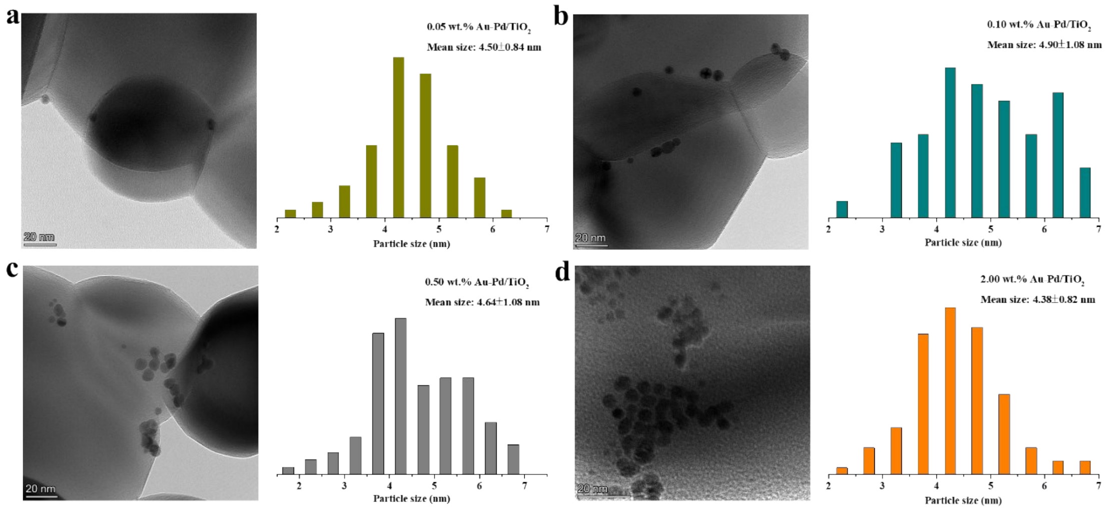

Fig. S3 TEM images of Au-Pd/TiO_2 with various Au-Pd loading amounts (0.05, 0.10, 0.50, and 2.00 wt.%) and their size distributions.

4. Mott-Schottky plot

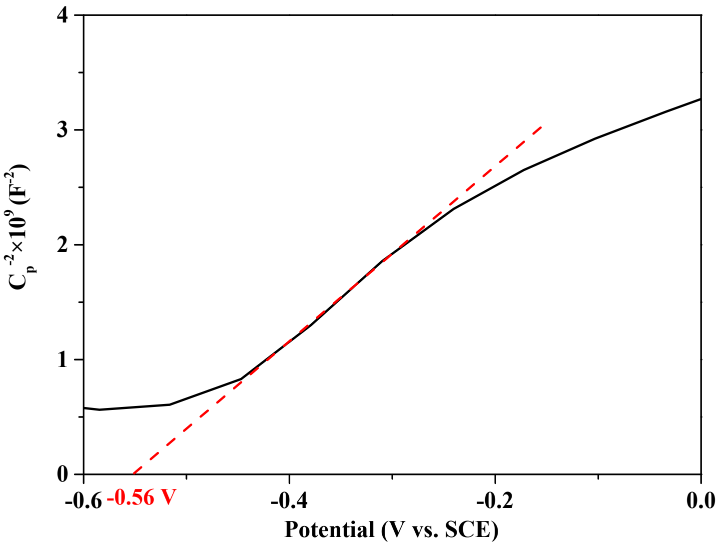

Fig. S4 Mott-Schottky plot of Au-Pd/TiO_2 recorded at 1000 Hz.

5. Electron paramagnetic resonance spectra

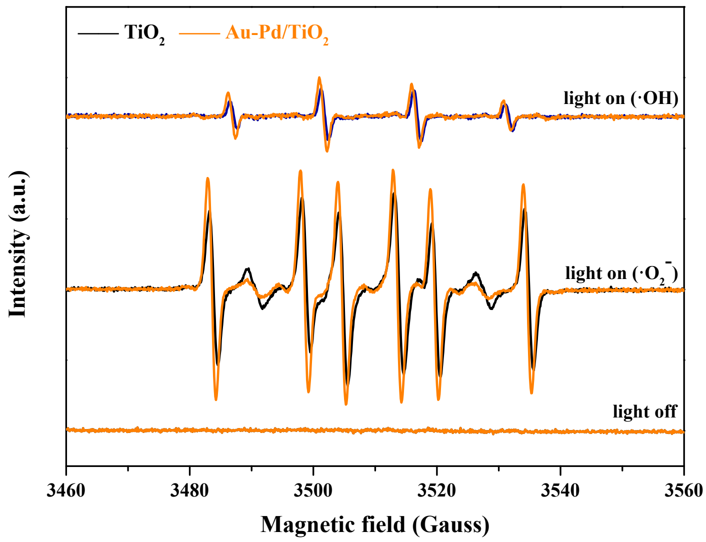

Fig. S5 EPR spectra of the catalyst suspension with 5,5-dimethyl-1-pyrroline N-oxide (DMPO) as the spin probe.

6. Photocatalytic methane oxidation under various partial pressures

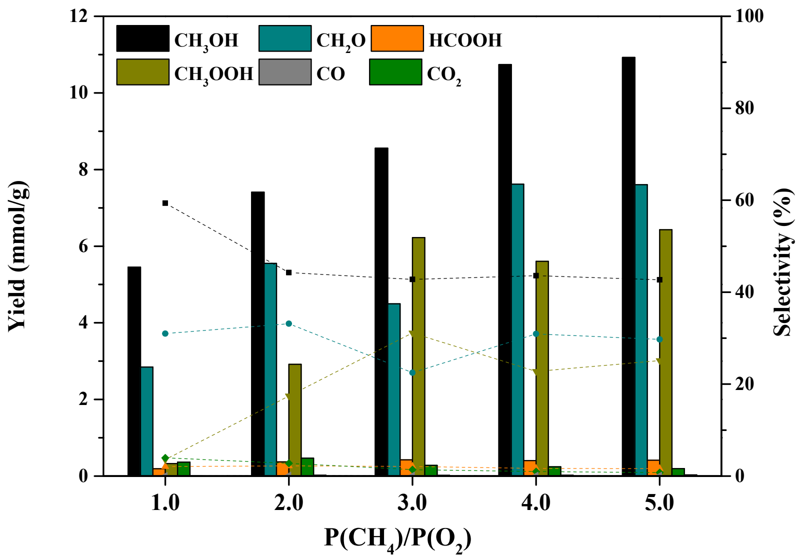

Fig. S6 Photocatalytic methane oxidation over Au-Pd/TiO_2 under various partial pressures under UV-visible light irradiation (5 mg catalyst, 30 mL water, 1.0-5.0 MPa CH_4, 1.0 MPa O_2, 1 h reaction).

7. Reported photocatalytic activities of methane conversion into methanol

Table S1. Reported photocatalytic activities of methane conversion into methanol.

Catalyst	Oxidant	Pressure or flowrate	Temp. (ºC)	Light source	Yield (μmol/g·h)	Selectivity	Ref.
V-MCM-41	NO	0.0006 MPa CH_4	22	100 W leg lamp > 270 nm	3.35	88.4%	1
NiO	H_2O	dissolved CH_4	25	high-power laser 355 nm	289	-	2
TiO_2					429	-	
WO_3					529	-	
Ag_2O/WO_3					2598	-	3
beta zeolite (HBEA)	H_2O	4.5 mL/min CH_4 17.9 mL/min He	70	medium-pressure mercury lamp	10	2.4%	4
V-HBEA					11.3	5.3%	
Bi-V-HBEA					10.7	6.4%	
V-HBEA				medium-pressure mercury lamp with UV-cut filter	2.7	81.6%	
Bi-V-HBEA					3.3	100%	
$BiVO_4$ thin platelet	H_2O	10% CH_4 in Ar	65	350 W xenon lamp	65.7	58.2%	5
$BiVO_4$ thick platelet					79.2	85.7%	
$BiVO_4$ bipyramid					111.9	85%	
$BiVO_4$	H_2O	4.5 mL/min CH_4 17.9 mL/min He	55	medium-pressure mercury lamp	19.9	42%	6
	1 mM NO_2^-				11.0	100%	
Bi_2WO_6 flower	H_2O				15.6	29.3%	7
Bi_2WO_6/TiO_2	H_2O				10.8	7.9%	
$BiVO_4$ platelet	H_2O				20.8	51%	
F/WO_3	H_2O				7.9	17.9%	8
La/WO_3	H_2O				31.4	46%	9
mesoporous WO_3	H_2O				27.2	46%	10
	2 mM Fe^{3+}				55.5	37.4%	
	0.1 mM Cu^{2+}				45.7	30.4%	
	2 mM Ag^+				16.5	11.8%	
	2 mM H_2O_2				20.3	34.3%	
FeO_x/TiO_2	0.8 mM H_2O_2	70 μmol CH_4 in Ar	25	300 W xenon lamp with 710-nm filter	352	90%	11
FeOOH/m-WO_3	1.5 mM H_2O_2	0.01 MPa CH_4	25	300 W xenon lamp 420-780 nm	239	91%	12
g-C_3N_4@$Cs_{0.33}WO_3$	O_2	pure air containing 1000 ppm CH_4	25	300 W xenon lamp	4.38	51.6%	13
$CuMoO_4/SiO_2$	O_2	CH_4:O_2 = 9:1	100	1000 W xenon lamp	15	-	14
MoO_4/SiO_2					5		
silica gel	O_2 (H_2O)	0.05 MPa CH_4	25	mercury lamp 185 nm	948	52.1%	15
silicalite					1597	46.5%	
beta (Si F)					1917	50.7%	
beta (Al F)					3604	49.8%	
beta (Si OH)					4284	48.0%	
beta (Al OH)					3965	54.9%	
Quantum-sized $BiVO_4$	O_2 (H_2O)	1.0 MPa CH_4 1.0 MPa O_2	30	xenon lamp 400-780 nm	367	96.6%	16
Au/black phosphorus	O_2 (H_2O)	3.0 MPa CH_4 0.3 MPa O_2	90	xenon lamp	57	99%	17
TiO_2	O_2 (H_2O)	0.0045 MPa CH_4 0.0005 MPa O_2 0.0050 MPa He	60	250 W high-pressure mercury lamp	7	1.57%	18
Mo/TiO_2					12.5	1.41%	
Au-CoO_x/TiO_2	O_2 (H_2O)	2.0 MPa CH_4 0.1 MPa O_2	25	300 W xenon lamp 300-500 nm	1500	57%	19
Pt/ZnO					2225	19.1%	20
Pd/ZnO					3035	26.2%	
Au/ZnO					2060	15.7%	
Ag/ZnO					365	5%	
Au/ZnO	O_2 (H_2O)	1.5 MPa CH_4 0.5MPa O_2	30	xenon lamp	686	99%	21
Au-Pd/TiO_2	O_2 (H_2O)	3.0 MPa CH_4 1.0 MPa O_2	42	xenon lamp	8557 (30 mL H_2O)	42.8% (30 mL H_2O)	this work
					12556 (50 mL H_2O)	42.3% (50 mL H_2O)	

8. Composition of O1s X-ray photoelectron spectra

Table S2. Binding energies and atomic ratios of lattice oxygen (O_L), oxygen from surface hydroxyl (O_H), and oxygen from adsorbed water (O_W).

Sample	O_L	O_H	O_W
Bare TiO_2	529.80 (68.08%)	531.09 (8.84%)	532.10 (23.07%)
Au/TiO_2	530.06 (78.91%)	531.13 (10.23%)	532.23 (10.86%)
Pd/TiO_2	529.82 (87.58%)	530.97 (5.55%)	532.27 (6.87%)
Au−Pd/TiO_2	529.81 (77.74%)	530.97 (14.53%)	532.31 (7.73%)

Reference

1. Y. Hu, M. Anpo and C. Wei, *J. Photochem. Photobiol., A* 2013, **264**, 48-55.
2. M. A. Gondal, A. Hameed, Z. H. Yamani and A. Arfaj, *Chem. Phys. Lett.* , 2004, **392**, 372-377.
3. A. Hameed, I. M. I. Ismail, M. Aslam and M. A. Gondal, *Appl. Catal., A*, 2014, **470**, 327-335.
4. S. Murcia-López, M. C. Bacariza, K. Villa, J. M. Lopes, C. Henriques, J. R. Morante and T. Andreu, *ACS Catal.*, 2017, **7**, 2878-2885.
5. W. Zhu, M. Shen, G. Fan, A. Yang, J. R. Meyer, Y. Ou, B. Yin, J. Fortner, M. Foston, Z. Li, Z. Zou and B. Sadtler, *ACS Appl. Nano Mater.*, 2018, **1**, 6683-6691.
6. S. Murcia-López, K. Villa, T. Andreu and J. R. Morante, *Chem. Commun.* , 2015, **51**, 7249-7252.
7. S. Murcia-López, K. Villa, T. Andreu and J. R. Morante, *ACS Catal.*, 2014, **4**, 3013-3019.
8. K. Villa, S. Murcia-López, T. Andreu and J. R. Morante, *Catal. Commun.* , 2015, **58**, 200-203.
9. K. Villa, S. Murcia-López, J. R. Morante and T. Andreu, *Appl. Catal., B* 2016, **187**, 30-36.
10. K. Villa, S. Murcia-López, T. Andreu and J. R. Morante, *Appl. Catal., B* 2015, **163**, 150-155.

11. J. Xie, R. Jin, A. Li, Y. Bi, Q. Ruan, Y. Deng, Y. Zhang, S. Yao, G. Sankar, D. Ma and J. Tang, *Nat. Catal.*, 2018, **1**, 889-896.
12. J. Yang, J. Hao, J. Wei, J. Dai and Y. Li, *Fuel*, 2020, **266**, 117104.
13. Y. Li, J. Li, G. Zhang, K. Wang and X. Wu, *ACS Sustain. Chem. Eng.*, 2019, **7**, 4382-4389.
14. M. D. Ward, J. F. Brazdil, S. P. Mehandru and A. B. Anderson, *J. Phys. Chem.*, 1987, **91**, 6515-6521.
15. F. Sastre, V. Fornés, A. Corma and H. García, *J. Am. Chem. Soc.* , 2011, **133**, 17257-17261.
16. Y. Fan, W. Zhou, X. Qiu, H. Li, Y. Jiang, Z. Sun, D. Han, L. Niu and Z. Tang, *Nat. Sustain.*, 2021, DOI: 10.1038/s41893-021-00682-x.
17. L. Luo, J. Luo, H. Li, F. Ren, Y. Zhang, A. Liu, W.-X. Li and J. Zeng, *Nat. Comm.*, 2021, **12**, 1218.
18. X. Chen and S. Li, *Chem. Lett.*, 2000, **29**, 314-315.
19. H. Song, X. Meng, S. Wang, W. Zhou, S. Song, T. Kako and J. Ye, *ACS Catal.*, 2020, **10**, 14318-14326.
20. H. Song, X. Meng, S. Wang, W. Zhou, X. Wang, T. Kako and J. Ye, *J. Am. Chem. Soc.* , 2019, **141**, 20507-20515.
21. W. Zhou, X. Qiu, Y. Jiang, Y. Fan, S. Wei, D. Han, L. Niu and Z. Tang, *J. Mater. Chem. A*, 2020, **8**, 13277-13284.